Mechanical micromodeling of stress-shielding at the bone-implant interphase under shear loading

Yoann Hériveaux, Sophie Le Cann, Manon Fraulob, Elsa Vennat, Vu-Hieu Nguyen, Guillaume Haïat

Mechanical micromodeling of stress-shielding at the bone-implant interphase under shear loading

Yoann Hériveaux[1], Sophie Le Cann[2], Manon Fraulob[2], Elsa Vennat[1], Vu-Hieu Nguyen[3], Guillaume Haïat[2]

Medical & Biological Engineering & Computing. https://doi.org/10.1007/s11517-022-02657-2
Received: 18 May 2022 / Accepted: 22 August 2022

1. Université Paris-Saclay, ENS Paris-Saclay, CentraleSupélec, CNRS, LMPS - Laboratoire de Mécanique Paris-Saclay, 91190, Gif-sur-Yvette, France.
2. CNRS, Laboratoire Modélisation et Simulation Multi Echelle, MSME UMR 8208 CNRS, 61 avenue du Général de Gaulle, 94010 Créteil Cedex, France.
3. MSME, CNRS UMR 8208, Univ Paris Est Creteil, Univ Gustave Eiffel, F-94010 Creteil, France

Inserting a titanium implant in bone tissue may modify its physiological loading and therefore cause bone resorption, *via* a phenomenon called stress-shielding. The local stress field around the bone-implant interphase (BII) created under shear loading may be influenced by different parameters such as the bone-implant contact (BIC) ratio, the bone Young's modulus, the implant roughness and the implant material. To evaluate their impact, a 2-D finite element model was developed to model the BII. The implant roughness was described by a sinusoidal function (height 2Δ, wavelength λ) and different values of the BIC ratio were simulated. A heterogeneous distribution of the maximum shear stress was evidenced in the periprosthetic bone tissue, with high interfacial stress for low BIC ratios and low implant roughness, and underloaded regions near the roughness valleys. Both phenomena may lead to stress-shielding related effects, which was concentrated within a distance lower than $0.8.\lambda$ from the implant surface. Choosing an implant material with mechanical properties matching those of bone tissue leads to a homogenized shear stress field, and could help to prevent stress-shielding effects. Finally, the equivalent shear modulus of the BII was derived to replace its complex behavior by a simpler analytical model in future studies.

Keywords: bone-implant interphase; shear loading; stress-shielding; osseointegration; finite element modeling

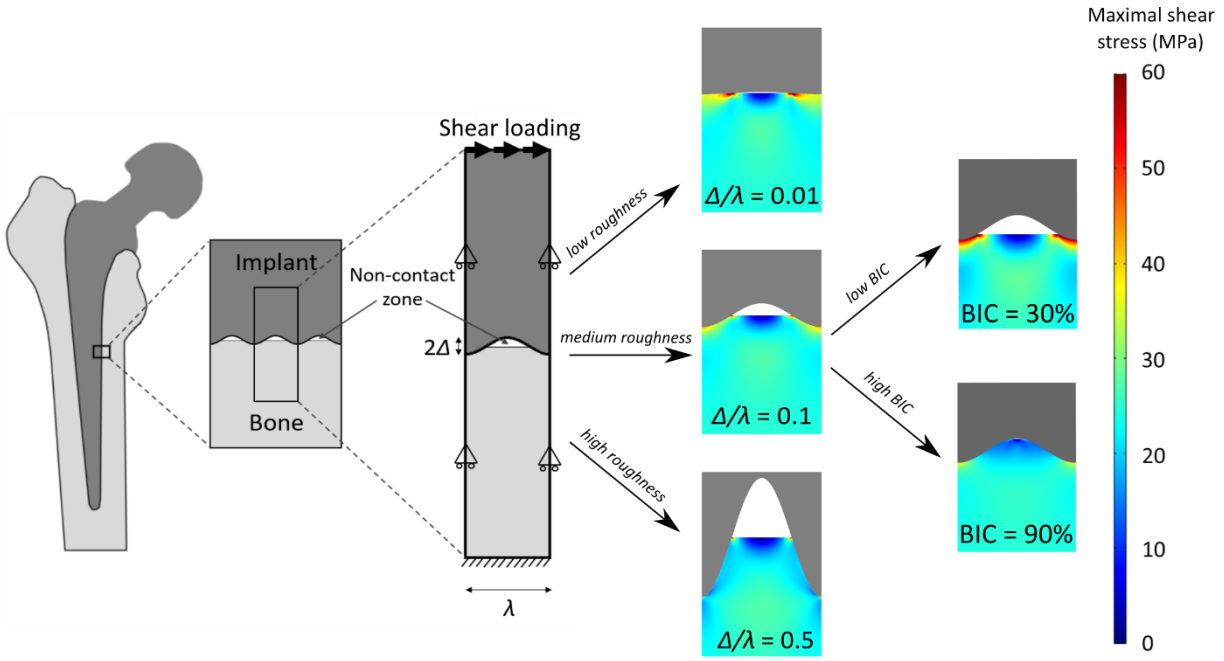

Graphical abstract: *Schematic illustrations of the 2-D finite element model used in the present study, and spatial variation of the maximal shear stress in periprosthetic bone tissue for different implant roughness and bone-implant contact ratios.*

1. Introduction

While endosseous cementless implants are now routinely used in dental, maxillofacial and orthopedic surgeries, implant failures still occur and may have dramatic consequences [36]. Implant stability determines the implant success and can be evaluated at two different stages. Primary stability is achieved directly after the surgery and depends mainly on the bone quality and on interlocking phenomena at the bone-implant interphase (BII). Secondary stability is achieved after a healing period through the osseointegration process, which corresponds to new bone formation and maturation in intimate contact with the implant [2]. Anticipating implant failures remains difficult due to the complex nature of the BII, and due to the evolution of the biomechanical properties of the BII [40]. As bone formation and remodeling are highly dependent on the mechanical environment perceived by the tissue, as stated by Wolff's law [17], they are affected by the presence of a stiff implant, and in turn, condition its integration.

Inserting a titanium implant in bone tissue induces a local modification of the physiological loading of bone tissue, especially at the vicinity of the implant, which could lead to bone loss via a phenomenon called stress-shielding [60]. Stress-shielding is directly related to the stress distribution in periprosthetic bone. While excessive stresses can damage the consolidating BII and lead to bone necrosis [11], loading is necessary to stimulate bone remodeling and avoid bone resorption [7]. Therefore, monitoring and preventing stress-shielding is especially important for load-carrying implants used in orthopedic applications such as total hip [6, 67] or knee [10, 68] arthroplasty.

Stress-shielding can be affected by various biomechanical factors, such as external loading [5, 66], the quality and quantity of periprosthetic bone tissue, or the implant material and geometrical design [51]. In particular, the use of biomaterials with lower mechanical properties than titanium alloys is currently explored in order to decrease the gap of mechanical properties between the implant and the bone [4, 47], which may help to reduce stress-shielding related effects. Furthermore, both the implant surface roughness [15, 55] and friction phenomena induced by non-perfect contact between the bone and the implant [28, 59] influence the stress distribution inside the periprosthetic bone, which in turn affects osseointegration phenomena. Investigating how these parameters affect stress-shielding is therefore of interest.

The mechanism precisely describing how stress-shielding can lead to bone resorption remains unclear. Retrieving information on the properties of the bone tissue at the scale of 1 to 200 µm from the implant surface remains difficult experimentally. In the clinics, implants follow-up is done via radiography [21, 29], which constitutes a global approach with limited resolution. Therefore, while periprosthetic bone loss associated with stress-shielding may be evidenced radiographically by performing 2-years or 5-years follow-ups [9, 12], clinical X-rays based techniques do not allow to characterize the BII at the microscopic scale, nor to explain the possible causes of stress-shielding. Acoustic methods [42, 64] as well as high resolution microtomography combined with mechanical loading [37, 69] have been developed to investigate the BII properties at the scale of tens of micrometers. However, such techniques require *in vivo*

experiments to generate biological interphase, are limited in case of complex implant geometries, and are destructive when mechanical testing is conducted. Interestingly, finite element (FE) modeling enables to control and investigate independently the parameters influencing the osseointegration of the BII, and is therefore a promising approach to provide clear-cut explanation on the basic phenomena related to stress-shielding.

The influence of the implant mechanical properties and of its macroscale design on the stress field around the implant has been extensively studied through numerical simulations at the macroscale [22, 45, 57] but only few studies investigated the BII microscale response. Moreover, most numerical simulations consider a fully bounded BII [18, 35, 43], without taking into account the effect of the implant surface roughness and of the partial contact area between the implant and bone tissue. It would be interesting to replace a fully bounded BII by an equivalent interphase, that would allow to consider the microscopic properties of the BII at the macroscale without increasing significantly computation times.

Recently, different analytical models have been proposed to describe the behavior of an osseointegrated BII under tensile [52] or dynamic [24] loadings. Korabi et *al.* [33] considered the dental implant-jawbone system and introduced a concept of failure envelope to assess the influence of the implant stiffness on possible strain- and stress-shielding. A previous paper by our group [53] examined the effects of changes of the implant surface roughness, of the bone-implant contact (BIC) ratio and of the properties of periprosthetic bone tissue on the variations of the stress field surrounding a BII under tensile loading. However, to the best of our knowledge, no study has so far investigated the effect of a shear loading on the mechanical behavior of the BII, although shear loading is an important loading mode in implantology. The loading conditions are known to impact the mechanical response of the BII in orthopedic applications, *eg.* for hip [65], femoral [20] or tibial implants [8]. A significant influence of a shear loading on the micromotions occurring at the BII was evidenced in these studies, which in turn impacts the stability of the implant [32]. Moreover, the interfacial shear stress was shown to be correlated with stress-shielding phenomena in hip prosthesis [31]. Investigating how a shear loading may affect stress-shielding is therefore of clinical and biomechanical interest.

The aim of the present work is to investigate the influence of different parameters describing the bone-implant interphase (BII) - namely the bone-implant contact (BIC) ratio, the implant roughness and the implant material - on the local stress field around the BII under shear loading. To do so, a 2-D FE model of the BII was developed to determine the maximum shear stress in the periprosthetic bone tissue for different BII configurations. The equivalent shear modulus of the interphase was also derived from these simulations, which will allow to replace the complex behavior of the BII by a simpler model corresponding to an equivalent interphase model.

2. Material and methods

2.1. Modeling of the bone-implant interphase

a. Geometry

The 2D model considered herein derives from the one developed in Raffa et *al*. [53], where the tensile behavior of the bone-implant interphase (BII) was investigated. Here, a shear loading is applied to the BII by considering two half-spaces corresponding to a rough implant and to cortical bone tissue respectively, separated from each other by a rough interphase (see Fig. 1).

Similarly to what was done in previous studies [25, 26, 53], the implant roughness was modeled by a sinusoidal function *s(x)* (coordinate system (O*xy*) shown in Fig. 1b) of amplitude 2Δ and of wavelength λ and given by:

$$\boldsymbol{s(x) = \Delta\left[1 - \cos\left(\frac{2\pi x}{\lambda}\right)\right].} \qquad \boldsymbol{x \in [0, \lambda]} \qquad \text{(Eq. 1)}$$

Preliminary computations with different values of λ and Δ but same ratio Δ/λ, so-called the waviness ratio, were shown to give identical results, which can be explained by the dimensionless nature of the model. Therefore, this waviness ratio Δ/λ was considered as the parameter to describe the implant surface profile. A fixed value of Δ equal to 5 µm was considered in the rest of the study, and λ was varied between 10 µm and 500 µm to simulate waviness ratios Δ/λ between 0.01 and 0.5 corresponding to two different scales of implant roughness [3].

A bone level parallel to the *x*-axis and delimiting a non-contact zone was introduced to simulate different values of the bone-implant contact (BIC) ratio. Numerical simulations were performed for BIC ratios between 5% and 95% by adjusting the ordinate (y-axis) of this interfacial line.

The total height of the model along the *y*-direction 2*H* = 8 mm was chosen large enough so that the spatial variation of the stress field around the BII was not influenced by the boundary conditions at the top (*y* = *H*) and at the bottom of the model (*y* = -*H*). The height of the implant domain (respectively the bone tissue domain) was chosen equal to *H* - 2Δ (respectively *H*), as represented in Fig 1b.

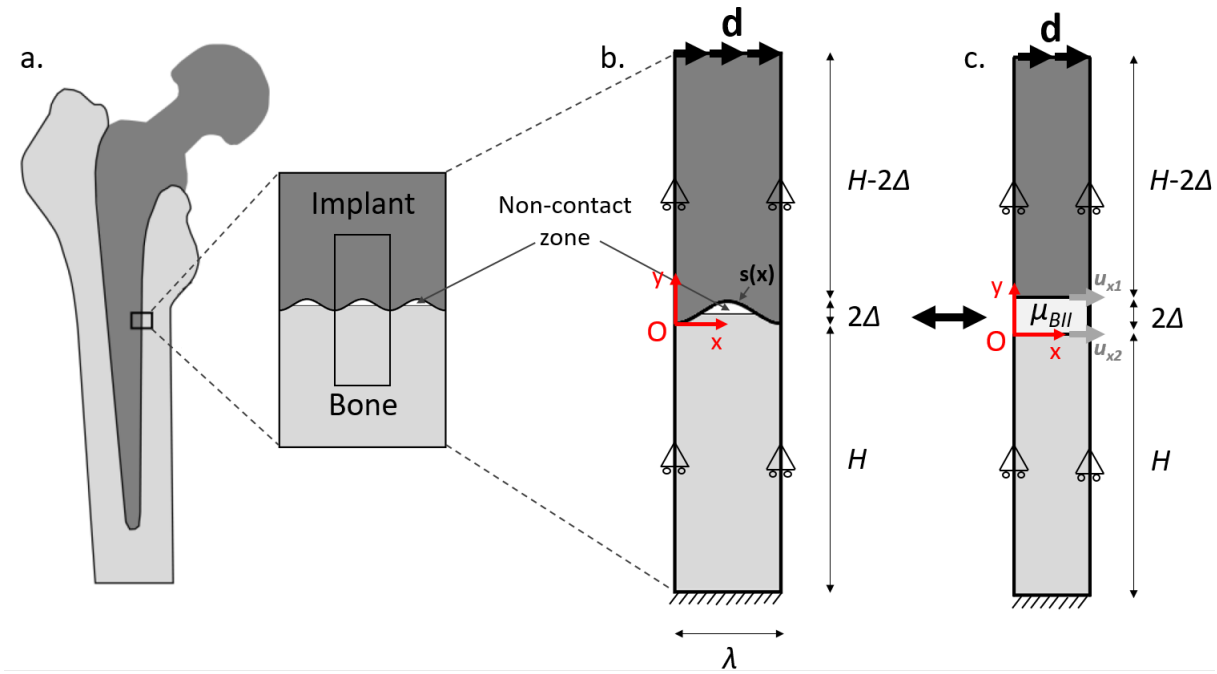

Fig. 1: *Schematic illustrations of the 2-D FE model used in the present study. (a) Example of a macroscopic description, corresponding to a femoral stem with a zoom-in depicting the geometrical description of the rough bone-implant interphase. (b) Detail of the geometrical model: the sinusoidal function s(x) to model the implant roughness (amplitude 2Δ, wavelength λ), the periodical boundary conditions (along the y-axis), the non-contact zone to model various BIC conditions and the applied displacement d on the implant. (c) Equivalent analytical model used to replace the BII by an equivalent interphase with shear modulus* μ_{BII}.

b. Materials

All materials were assumed to be linear-elastic and to have homogeneous isotropic mechanical properties. For the bone domain, mature cortical bone with a Young's modulus value of E_b = 20 GPa was considered as a reference [44], and less mature bone configurations (1 to 10 GPa) were also simulated, to investigate the temporal evolution of the material properties during healing [14, 38]. The impact of the implant's material properties on stress shielding phenomena was investigated *via* two different materials employed in orthopedic applications: a reference Titanium alloy (Ti-6Al-4V) with a Young's modulus E of 113 GPa [46] and a metal-polymer composite (Ti-35BPA) with E = 20 GPa [49]. All materials had a Poisson ratio ν equal to 0.3.

c. Boundary conditions

Boundary conditions were introduced to describe a shear loading of the bone-implant interphase. To do so, an arbitrary displacement $u_x = d$ = 15 µm (Fig. 1b) was uniformly applied at the top of the implant subdomain ($y = H$), inducing locally a shear stress τ_0 between 20 MPa and 25 MPa (depending on the tested configurations), which correspond to levels of loading shown to enhance bone remodeling around implants [58]. At the bottom of the model ($y = -H$), a fixed boundary condition was set ($u_x = u_y = 0$). Note that due to the linear assumptions of the model, the amplitude of the stress field within the periprosthetic bone is directly proportional to the value of d.

Due to the periodicity of the problem, a simplified model of a single sine period of the interphase was considered (see Fig. 1c), in which anti-symmetrical boundary conditions were set on the vertical boundaries : $u_y = 0$ at $x = 0$ and at $x = \lambda$

A perfect contact condition was assumed where the bone and the implant were in contact, with the continuity of displacement and normal stress fields at the contacting surfaces between bone and implant.

d. Finite element simulation

The static linear elastic problem was solved using the FE method. All numerical analyses were carried out using Comsol Multiphysics® (Stockholm, Sweden). All subdomains were meshed with triangular quadratic elements. A convergence study was performed to determine the minimum element size, which was set equal to 2×10^{-7} m. The mesh size was refined surrounding the non-contact zone at the BII in order to better describe stress concentrations, in particular for lower values of Δ/λ. For the reference configuration corresponding to BIC = 50% and $\Delta/\lambda = 0.1$, we obtained 930,000 second-order triangular elements, leading to a global system with about 3,700,000 degrees of freedom.

2.2. Evaluation of the shear stress field

To explore the stress field in periprosthetic bone tissue, the maximal shear stress τ_{max} was chosen as the main parameter, calculated as follow (Eq. 2):

$$\boldsymbol{\tau_{max}}(\boldsymbol{x}, \tilde{\boldsymbol{y}}) = \frac{\boldsymbol{\sigma_{p1} - \sigma_{p3}}}{\mathbf{2}} \qquad \text{(Eq. 2)}$$

where $\tilde{y} = \frac{-y}{\lambda}$ is a non-dimensional coordinate, normalizing the distance from the implant surface, and $\sigma_{p1}$and σ_{p3} are the first and third principal stresses in bone tissue, respectively (with $\sigma_{p1} > \sigma_{p3}$). Note that a second non-dimensional coordinate $\tilde{x} = \frac{x}{\lambda}$ was also introduced in what follows to normalize the distance along the *x*-axis.

To evaluate the depth of the region of interest where the BII influences the stress distribution, the shear stress was averaged over *x*, for a given distance $\tilde{y}$ from the implant surface following:

$$\langle \boldsymbol{\tau_{max}} \rangle (\tilde{\boldsymbol{y}}) = \frac{\mathbf{1}}{\boldsymbol{\lambda}} \int_{\mathbf{0}}^{\boldsymbol{\lambda}} \boldsymbol{\tau_{max}}(\boldsymbol{x}, \tilde{\boldsymbol{y}})\, \boldsymbol{dx} \qquad \text{(Eq. 3)}$$

To evaluate the spatial distribution of the stress field, the standard deviation of τ_{max} over *x* for a given $\tilde{y}$ was calculated as follows:

$$\boldsymbol{SD\tau_{max}}(\tilde{\boldsymbol{y}}) = \sqrt{\frac{\mathbf{1}}{\boldsymbol{\lambda}} \int_{\mathbf{0}}^{\boldsymbol{\lambda}} (\boldsymbol{\tau_{max}}(\boldsymbol{x}, \tilde{\boldsymbol{y}}) - \langle \boldsymbol{\tau_{max}} \rangle (\tilde{\boldsymbol{y}}))^2\, \boldsymbol{dx}} \qquad \text{(Eq. 4)}$$

To evaluate the impact of using the metal-polymer composite (Ti-35BPA) compared to the reference titanium alloy as the implant material, the difference between the normalized values of τ_{max} obtained with both materials was calculated (Eq. 5), and its spatial variation was investigated.

$$\Delta\tau_{max}(x,\tilde{y}) = \frac{\tau_{max}^{BPA}(x,\tilde{y})}{\tau_0^{BPA}(x,\tilde{y})} - \frac{\tau_{max}^{Ti}(x,\tilde{y})}{\tau_0^{Ti}(x,\tilde{y})} \qquad \text{(Eq. 5)}$$

where $\tau_{max}^{Ti}(x,\tilde{y})$ (respectively $\tau_{max}^{BPA}(x,\tilde{y})$) corresponds to the maximum shear stress in bone tissue when the implant is made of Titanium alloy (respectively Ti-35BPA). Similarly, τ_0^{Ti} (respectively τ_0^{BPA}) represents the shear stress at the top of the implant domain when the implant is made of Titanium alloy (respectively Ti-35BPA).

2.3. Equivalent model of the interphase

A simple three-layer 2D model was developed to assess the equivalent shear modulus of the BII (Fig. 1c). The top layer (y > 2Δ) represents the implant subdomain and the bottom layer (y < *0*) the bone one. Both implant and bone subdomains have the same properties as in the numerical model (see section 2.1). The medium layer (y $\in [0\,;2\Delta]$) corresponds to the interphase and was assumed to have homogeneous mechanical properties and a shear modulus equal to μ_{BII}, depending on the waviness ratio Δ/λ, the BIC ratio and the material properties of the bone and of the implant.

The displacement field in each subdomain was assumed to be constant with respect to *x* and vary linearly with respect to *y*, so that its component along the *x* direction writes:

$$u_x(y) = \begin{cases} d + \frac{(d-u_{x1})}{H-2\Delta}(y-H) & \text{for } y > 2\Delta \quad \text{(Implant)} \\ u_{x2} + \frac{(u_{x1}-u_{x2})}{2\Delta}y & \text{for y} \in [0\,;2\Delta] \quad \text{(Interphase)} \\ \frac{u_{x2}}{H}(y+H) & \text{for y} < 0 \quad \text{(Bone)} \end{cases} \qquad \text{(Eq. 6)}$$

where u_{x1} and u_{x2} represent the displacements at both extremities of the interphase, respectively at $y = 2\Delta$ and $y = 0$ (see Fig 1c). Therefore, in each layer, the shear stress σ_{xy} is given by:

$$\sigma_{xy} = \mu\frac{\partial u_x}{\partial y} = \begin{cases} \mu_i \frac{d-u_{x1}}{H-2\Delta} & \text{for y} > 2\Delta \\ \mu_{BII}\frac{(u_{x1}-u_{x2})}{2\Delta} & \text{for y} \in [0\,;2\Delta] \\ \mu_b \frac{u_{x2}}{H} & \text{for y} < 0 \end{cases} \qquad \text{(Eq. 7)}$$

where μ is the shear modulus of the considered medium, namely μ_i for the implant, μ_{BII} for the interphase (unknown) and μ_b for cortical bone. The continuity of σ_{xy} at the interfaces of the different subdomains imposes:

$$\sigma_{xy} = \mu_i\frac{d-u_{x1}}{H-2\Delta} = \mu_{BII}\frac{(u_{x1}-u_{x2})}{2\Delta} = \mu_b\frac{u_{x2}}{H} = \tau_0 \qquad \text{(Eq. 8)}$$

where τ_0 is the shear stress imposed at the top of the implant layer.

Therefore, μ_{BII} can be expressed by:

$$\mu_{BII} = \frac{2\Delta}{\frac{d}{\tau_0} - \frac{(H-2\Delta)}{\mu_i} - \frac{H}{\mu_b}} \qquad \text{(Eq. 9)}$$

Numerical simulations were performed for different values of BIC, Δ/λ, and material properties, and the shear modulus of the interphase μ_{BII} was then derived from (Eq. 9).

3. Results

3.1. Effect of the implant roughness

When applying shear loading to the sinusoidal interphase model, shear stresses are not homogeneously distributed and concentrate in the bone tissue directly in contact with the implant (Fig. 2). The values of τ_{max} may exhibit local singularities at the intersection between the implant, the void and the bone, and local maxima at the roughness peaks ($\tilde{x} = 0$ and $\tilde{x} = 1$). Higher shear stress concentrations along the bone-implant boundary are evidenced for lower values of Δ/λ (Fig 2 left). Moreover, while τ_{max} is mostly higher than or of the same amplitude as the imposed shear load (τ_0~ 24.5 MPa here), the non-contact region (around $\tilde{x}$ = 0.5) is submitted to lower shear stresses (τ_{max} < 5 MPa, dark blue regions in Fig. 2a) in the vicinity of the implant. At higher distances from the implant, a local maximum of τ_{max} (around 30 MPa) is evidenced for $\tilde{x}$ = 0.5.

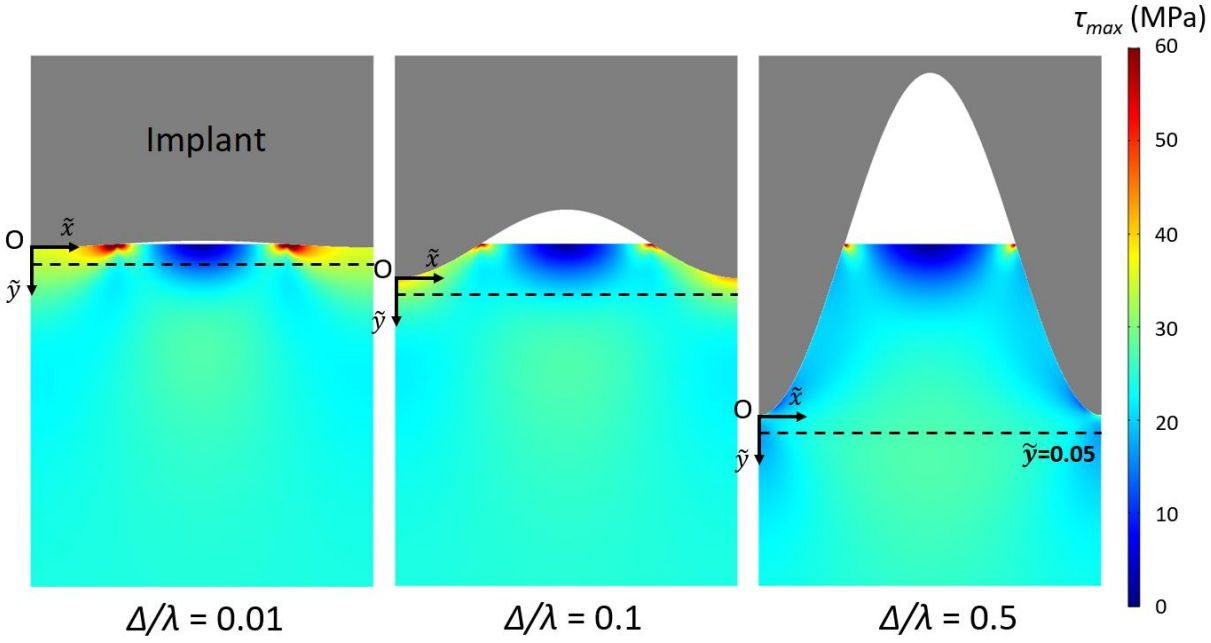

Fig. 2: *Spatial variation of the maximal shear stress τ_{max} around the BII for BIC = 50% and three waviness ratios Δ/λ = 0.01, 0.1, and 0.5. The reference material properties are: $E_{implant}$ = 113 GPa and E_{bone} = 20 GPa. Dotted lines correspond to the position $\tilde{y}$ = 0.05.*

To investigate the effect of the waviness ratio Δ/λ on stress-shielding phenomena, we studied the stress distribution in the bone tissue at $\tilde{y}$ = 0.05 (Fig. 3), a trade-off distance far enough from the BII to avoid too

localized effects, and close enough to still observe the influence of the BII. τ_{max} presents higher spatial variations for lower values of Δ/λ (dotted curves in Fig. 3), which are consistent with the spatial distributions shown in Fig 2. In particular, the stress concentration evidenced at the intersections between the void, the implant and the bone (Fig 2), are expressed as a local variation of τ_{max} at $\tilde{x}$ = 0.25 and 0.75 (Fig 3), which correspond to the positions of these intersections for a BIC ratio equal to 50%. The effect of this stress concentration is particularly clear for Δ/λ = 0.01, the lowest waviness ratio configuration, and to a lower extent for Δ/λ = 0.1.

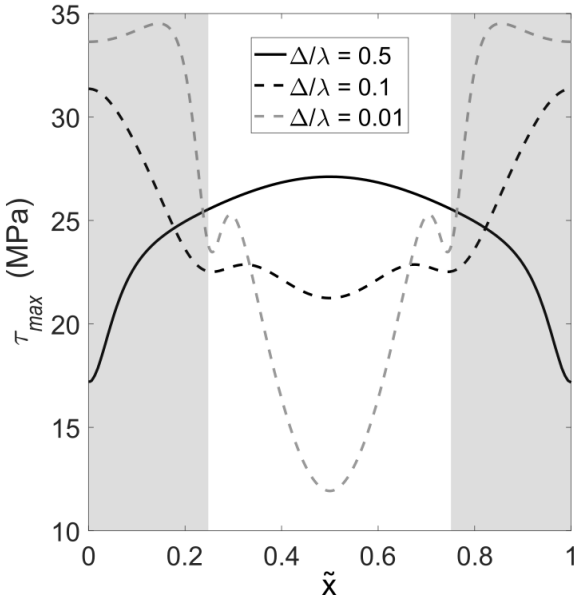

Fig. 3*: Variation of the maximal shear stress τ_{max} at $\tilde{y}$ = 0.05 (see Fig 2) over one sine period. Three values of the waviness ratio Δ/λ = 0.01, 0.1, and 0.5 are considered. The BIC ratio is equal to 50% and the reference material properties are: $E_{implant}$ = 113 GPa and E_{bone} = 20 GPa. The grey background corresponds to the $\tilde{x}$ values for which bone is in contact with the implant (i.e. $\tilde{x} < 0.25$ and $\tilde{x} > 0.75$).*

To investigate the spatial variation from the implant surface towards the bone tissue and to evaluate the region of interest where the presence of the BII influences the stress distribution, the values of τ_{max} were averaged along *x*, for various $\tilde{y}$ positions and different values of the waviness ratio (Fig. 4). The averaged normalized maximum shear stress ($\langle\tau_{max}\rangle/\tau_0$) decreases as a function of Δ/λ. While the averaged value $\langle\tau_{max}\rangle$ remains closed to τ_0 (+/- 2% τ_0) for all values of Δ/λ at a distance $\tilde{y} > 0.1$ (Fig. 4a), its standard deviation $SD\tau_{max}$ remains higher than 2% until a value of $\tilde{y} < 0.8$ (Fig. 4b). This result is consistent with Fig 2, which shows that the distribution of τ_{max} remains heterogeneous for $\tilde{y} > 0.1$.

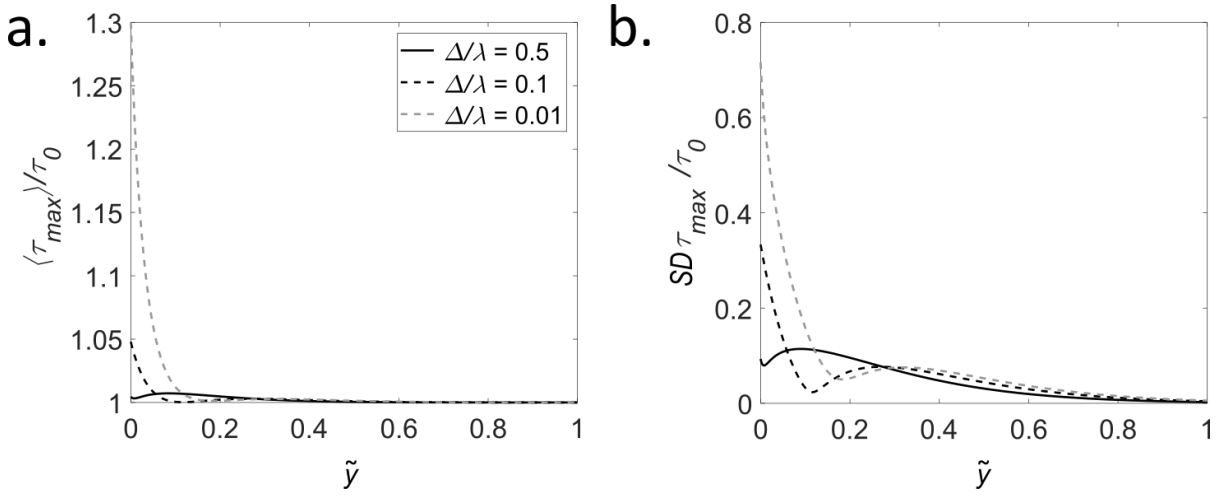

Fig. 4*: Variation of (a) the normalized maximum shear stress $\langle\tau_{max}\rangle/\tau_0$ averaged over x and (b) the standard variation of τ_{max}/τ_0 over x as a function of the normalized depth $\tilde{y}$ for different values of the waviness ratio Δ/λ. The BIC ratio is equal to 50% and the material properties are the reference ones ($E_{implant}$ = 113 GPa and E_{bone} = 20 GPa).*

3.2. Effect of the BIC ratio

To explore the effect of the bone-implant contact (BIC) ratio on the transmission of shear stress at the BII, different BIC ratios were considered with a fixed waviness ratio of $\Delta/\lambda = 0.1$ (Fig 5). Similarly as in Fig 2, the bone in direct contact with the implant is locally submitted to a shear stress higher than τ_0 (regions in red in Fig 5), while the shear stress is lower around $\tilde{x} = 0.5$ (regions in blue in Fig 5). The shear stress is particularly low around $\tilde{x} = 0.5$ for low BIC ratios, for which significant spatial variations of τ_{max} are also evidenced further away from the BII (*e.g.* for $\tilde{y} > 0.05$). On the contrary, the shear stress distribution tends to be more homogeneous for higher BIC ratios, in particular for BIC = 90%.

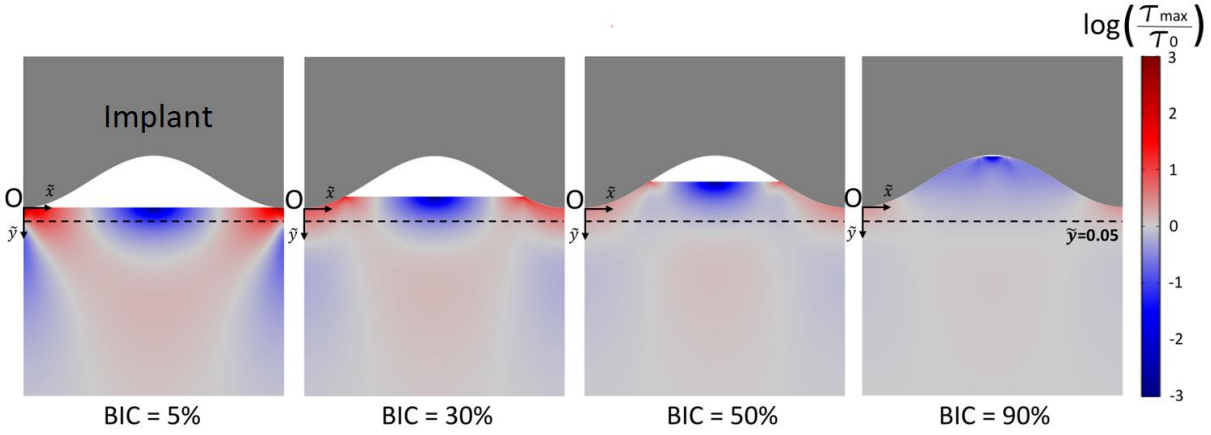

Fig. 5: *Spatial variation (logarithmic scale) of the normalized maximal shear stress τ_{max}/τ_0 around the BII for a waviness ratio $\Delta/\lambda = 0.1$ and four values of the BIC = 5%, 30%, 50% and 90%. The material properties are the reference ones ($E_{implant}$ = 113 GPa and E_{bone} = 20 GPa). Dotted lines correspond to the position $\tilde{y} = 0.05$.*

To investigate until which distance from the implant the BIC ratio influences the stress distribution, the shear stress was averaged along *x* at different $\tilde{y}$ positions, for a fixed waviness ratio of Δ/λ = 0.1 and different BIC ratios (Fig. 6). The normalized maximum shear stress (Fig 6a) decreases when the BIC ratio increases, up to an approximate distance $\tilde{y} = 0.1$. However, similarly as for the effect of the waviness ratio (Fig 4a), the standard deviation of τ_{max} over *x* at a given distance $\tilde{y}$ remains significant (>2% τ_0) until $\tilde{y} = 0.8$ (Fig. 6b).

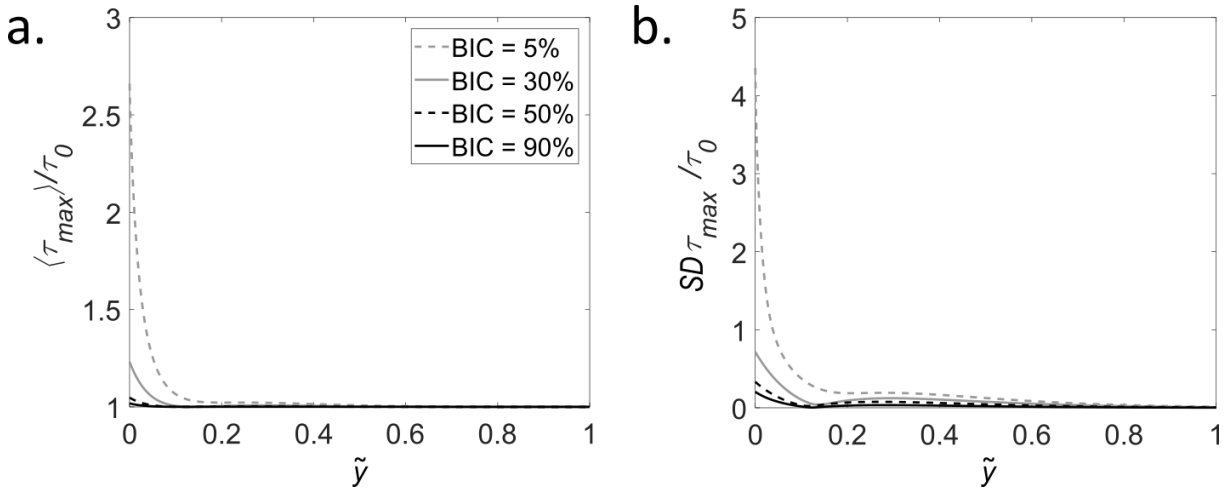

***Fig. 6**: Variation of (a) the normalized maximum shear stress $\langle\tau_{max}\rangle/\tau_0$ averaged over x and (b) the standard variation of τ_{max}/τ_0 over x as a function of the normalized depth ỹ for different values of the BIC. The waviness ratio is Δ/λ = 0.1 and the material properties are the reference ones ($E_{implant}$ = 113 GPa and E_{bone} = 20 GPa).*

3.3. Effect of the implant material

Replacing the reference Titanium alloy by a less stiff biomaterial (Ti-35BPA) leads to significant modifications of the distribution of τ_{max} (Fig. 7), especially for high implant roughness and high BIC ratios. In particular, for Δ/λ = 0.5 and BIC = 90%, τ_{max} increases by around 0.5 τ_0 in the region around $\tilde{x}$ = 0.5 and in proximity with the implant, a region which was under-loaded when using the reference Titanium alloy (see Fig 2 and 5). This increase of τ_{max} results in a more homogeneous stress distribution within the periprosthetic bone tissue for BIC = 90%, and to values of maximal shear stress slightly higher than τ_0 for Δ/λ = 0.5 when using Ti-35BPA (data not shown). Using a less stiff biomaterial therefore leads to a better transmission of shear stress at the BII for high waviness ratios and for high BIC ratios, which could help to prevent stress-shielding related effects. To a lower extent, the region where the stress field amplitude is lower is also reduced for the reference configuration (Δ/λ = 0.1 and BIC = 50%). However, for low implant roughness (Δ/λ = 0.01) and low BIC ratios (BIC = 5%), the change of implant material has relatively low and localized effects.

A decrease of interfacial stress is also evidenced in periprosthetic bone in direct contact with the implant for all configurations except for Δ/λ = 0.5, which corresponds to a situation where interfacial stresses are

already low (see Fig 2, right). However, the localized shear stress at the intersection between the implant, the void and the bone, which already corresponds to the maximal value of τ_{max} for the reference Titanium alloy, is further increased when using Ti-35BPA.

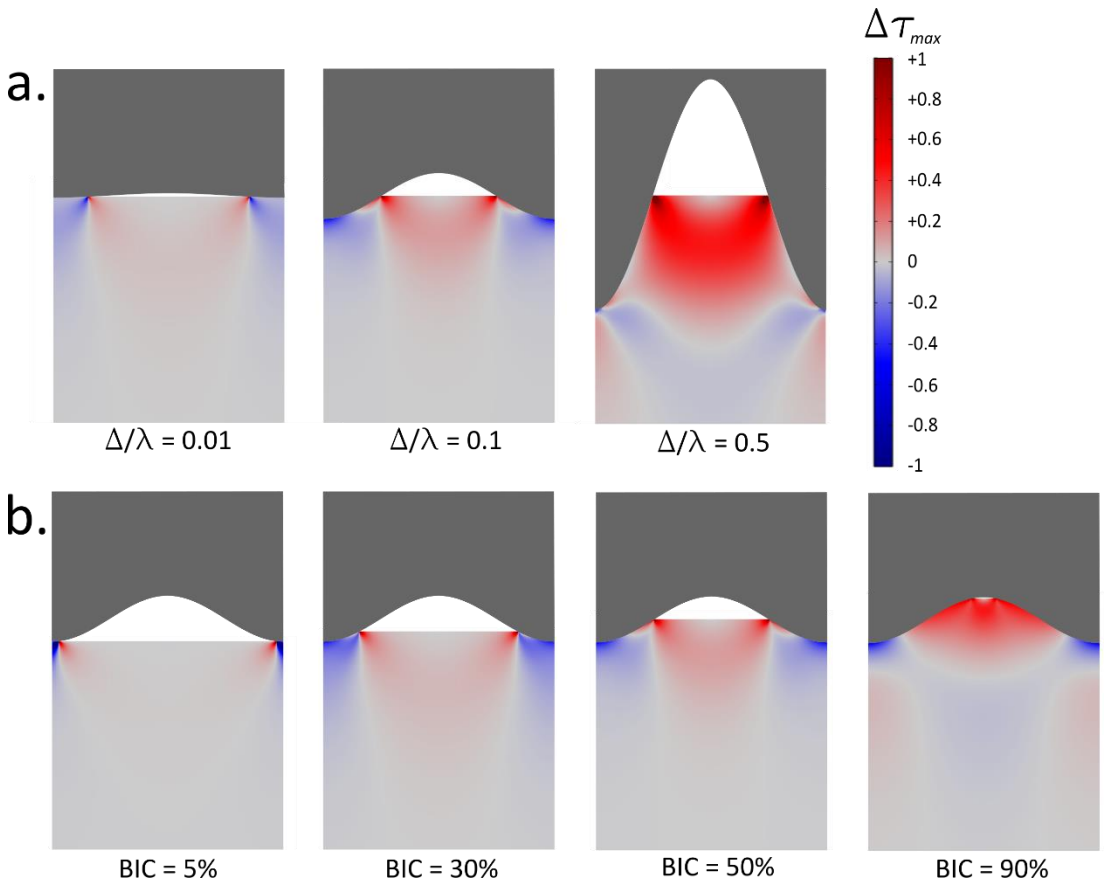

Fig. 7: *Spatial distribution of the difference $\Delta\tau_{max}$ between the maximal shear stress in bone tissue when using the metal-polymer composite Ti-35BPA (E=20 GPa) and the reference Titanium alloy (E=113 GPa) for the implant material. Simulations were performed (a): for a fixed BIC ratio of 50% and three waviness ratios Δ/λ = 0.01, 0.1 and 0.5, and (b) for a fixed waviness ratio Δ/λ = 0.1 and four values of the BIC = 5%, 30%, 50% and 90% (b), with E_{bone} = 20 GPa. Note that the configurations Δ/λ = 0.1 in Fig. 7a and BIC = 50% in Fig 7b correspond to the same data.*

3.4 Equivalent shear modulus of the bone-implant interphase

The interphase shear modulus μ_{BII} (as calculated from the equivalent model described in section 2.4) increases when the bone-implant contact (BIC) increases (Fig 8a,b), when the bone Young's modulus (E_b) increases (Fig 8b), as well as when the waviness ratio increases (Fig 8a). For given values of the BIC and of E_b, the interphase shear modulus μ_{BII} tends to vary less when reaching high values of Δ/λ, which correspond to large roughness (black curves in Fig 8a). Moreover, μ_{BII} is strongly influenced by variations of low BIC values for high values of Δ/λ, and on the contrary, by variations of large BIC for low values of Δ/λ (black *vs* grey curves in Fig 8a). The interphase shear modulus is also almost proportional to E_b (Fig 8b), so that for low values of E_b (1 GPa), values of μ_{BII} remain low.

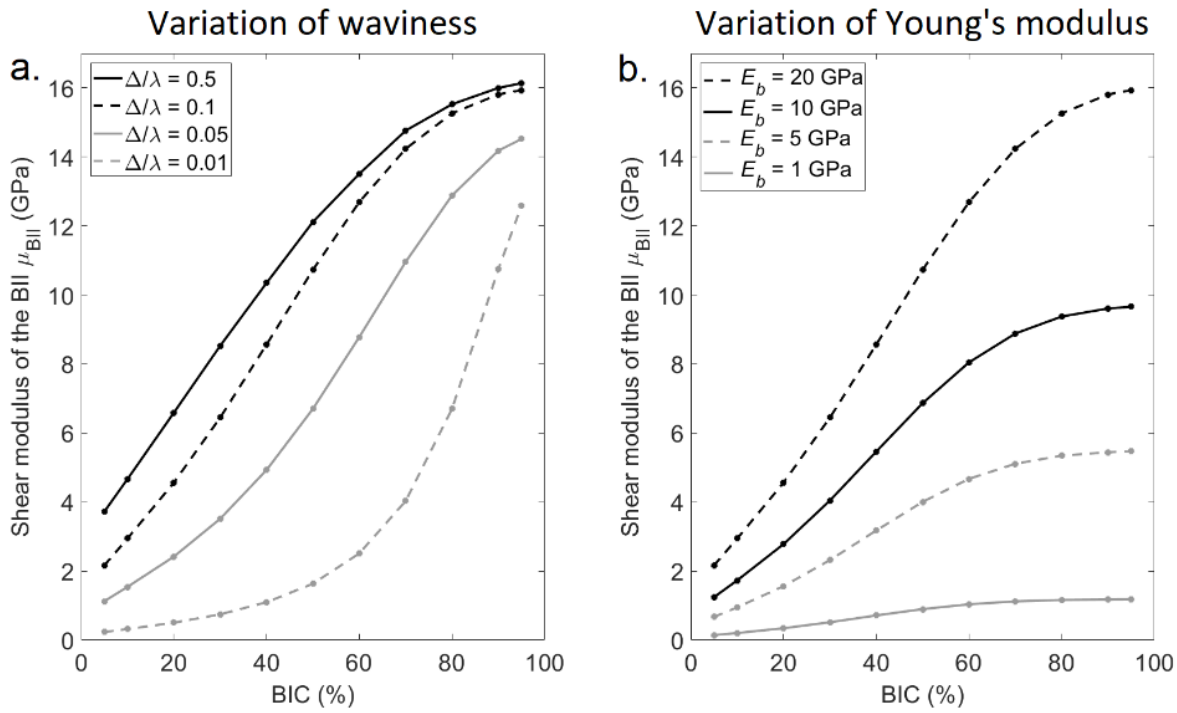

Fig. 8: *Variation of the shear modulus of the interphase μ_{BII} as a function of the BIC, (a) for different values of the waviness ratio Δ/λ and a fixed bone Young's modulus E_b of 20 GPa and (b) for different values of bone Young's moduli E_b and a fixed waviness ratio $\Delta/\lambda = 0.1$. The implant Young's modulus is taken as the reference (Titanium alloy), E = 113 GPa. Note that the black dotted lines correspond to the same configuration in Fig 8a and in Fig 8b.*

4. Discussion

The present study investigates numerically the spatial distribution of the stress field in bone tissue surrounding an implant subjected to a shear loading, and especially the effect of surface roughness, bone-implant contact and material properties, using a standardized sinusoidal model of a BII. The spatial distribution of the shear stress in the periprosthetic bone tissue was analyzed, and based on these results, a region of interest where the presence of an implant influences the local stress field was defined, which corresponds to the region where stress-shielding may occur.

The originality of this study is to consider the specific case of a shear loading, which was shown to significantly influence micromotions at the BII [8, 20, 65], and to investigate stress-shielding effects at the micro-scale, while most studies in the literature only focus on the macro-scale, *i.e.* on the whole implant geometry.

Maximal shear stresses obtained herein are higher than 100 MPa for some specific configurations (in particular low BIC ratios and low roughness) and are therefore higher than typical shear strength values of human cortical bone, which are around 50 MPa along the bone axis [61, 62]. Such levels of shear stress could thus potentially locally damage periprosthetic bone tissue and lead to bone resorption. However,

these maximum values were obtained for a given displacement of 15 µm, corresponding to shear loads between 20 and 25MPa, and hence may vary depending on the local geometrical configuration. Another potential explanation to the bone resorption phenomena associated to stress-shielding is related to the low stress region evidenced in bone tissue between two asperities of the implant roughness (Fig 2, around $\tilde{x}$ = 0.5), since the absence of mechanical solicitation is known to enhance bone resorption [13]. This decrease of the bone mechanical stimulation due to the implant acting as a shield was extensively reported in the literature at the macro-level, i.e. considering the whole implant geometry [27, 34] and seems to start at the micro-level, i.e. locally in between threads and local surface micro-roughness.

4.1. Effect of the implant roughness

The implant roughness was modelled *via* different values of waviness ratios Δ/λ, to account for the observed variability in the implant surface roughness studied in literature. Macroscopic roughness, *i.e.* related to the implant's geometrical design, was determined considering the specific case of dental implants. Macroscopic roughness structures can be accurately modeled by a sinusoidal surface because they present a threading. Rather high waviness ratios, ranging from 0.1 to 0.5, were chosen based on the depth (assimilated to 2Δ) and the pitch (λ) of typical implant threading [1, 39]. The case of microscopic surface roughness is more complex due to the lager variety of surface profiles. Some surface may present low waviness ratio (e.g. machined or polished surfaces), while others may indeed present higher waviness ratio (e.g. sandblasted with large alumina particles). The microscopic surface roughness of implants can be modulated with classical mechanical (*e.g.* sandblasting), chemical (*e.g.* acid-etching) or laser surface treatments, and is commonly characterized by the value of Ra (mean arithmetic roughness), typically comprised between 1 and tens of microns [3, 23, 56]. Although Δ corresponds to the roughness parameter *Rc*, we decided to use the parameter *Ra* because it is widely used in the implant literature [3]. Based on these values, waviness ratios between 0.01 and 0.1 were considered to model microscopic roughness, by assimilating Δ to $\pi.R_a$, and λ to S_m. However, high waviness ratios could still be observed at the micro-level, when considering highly abrasive methods such as sandblasting with large particles [3], which is also taken into account in the model.

The stress distribution at the BII is strongly dependent on the roughness of the implant. For low waviness (*i.e.* Δ/λ<0.1) a local concentration of the stress at the interphase is observed (Fig 2 and 3) whereas the stress distribution is more homogeneous when the waviness increases (*i.e.* Δ/λ = 0.5). This behavior can be explained by the presence of a stronger singularity at the tip of the non-contact zone in the low waviness configuration, which depicts a crack-like behavior. This engenders a high stress concentration at the tip, which is illustrated by a local increase of τ_{max} (Fig. 3) occurring for a *x* value corresponding to the position of the tip. Moreover, the direction of the shear loading with respect to the local interface shifts from almost parallel for Δ/λ = 0.01 to almost perpendicular for Δ/λ = 0.5, which explains that the shear stress level at the BII increases with Δ/λ due to a better stress transmission. Therefore, for a given BIC, the mechanical

strength of the BII is lower for low waviness ratio (low roughness), and depends essentially on adhesion phenomena.

The periodicity of the interphase λ has an impact on the depth at which the presence of the BII plays a role on the stress field. For different configurations, the stress fields remain heterogeneous until a distance of around 0.8 λ from the implant (Fig 4), which indicates that the region of interest where stress-shielding may occur directly depends on the implant roughness.

4.2. Effect of the temporal evolution of the BII during osseointegration

The temporal evolution of the BII during healing, which corresponds to osseointegration phenomena, can be modeled by an increase of the BIC ratio, which is often considered as the gold standard to assess implant stability [19]. The BIC is shown to affects the stress distribution around the BII (Fig 5 and 6). As the osseointegration proceeds and the BIC increases [30], the stress inside bone tissue progressively gets closer to the imposed stress at the implant surface, with a decrease of τ_{max} in bone tissue at the contact of the implant (overloaded regions) and an increase of the stress field around $\tilde{x}$ = 0.5 (underloaded regions, Fig 5), leading to a reduced stress-shielding. While τ_{max} may exceed the bone shear strength for a BIC ratio of 5% due to local singularities, the shear stress remains relatively homogeneous for a BIC ratio of 90% (Fig 6a). Therefore, this study emphasizes the importance of maximizing the BIC ratio for clinical success, as it can minimize stress-shielding phenomena (as shown herein) as well as improve implant stability [40].

Osseointegration is also associated with an increase of bone mechanical properties at the BII through the progressive maturation of bone tissue [63]. The influence of periprosthetic bone quality and quantity was investigated in this study through the estimation of the equivalent shear modulus of the BII, which increases when the BIC ratio increases and when the bone Young's modulus increases (Fig 8). The results are consistent with an increase of the BII stiffness during osseointegration, which was evidenced numerically in previous studies [24, 52].

The influence of the implant roughness and of the temporal evolution of the BII were investigated separately in the present study. However, these two properties are correlated since bone quantity and mechanical properties depend on the scale considered for the roughness. Based on experimental data, future studies should couple these simulations with bone remodeling algorithms at the microscopic scale, to consider the coupling of bone's adaptation with the surface roughness during osseointegration phenomena.

4.3. Effect of the implant material

Stress-shielding is also influenced by the gap in the material properties between the implant and the bone tissue. Previous studies highlighted that an ideal implant material should therefore combine the high

strength of metals with a low stiffness matching that of bone [47, 48]. The present study emphasizes that using implant materials with mechanical properties closer to those of the bone leads to a homogenization of the shear stress distribution, with a decrease of interfacial stress and an increase of shear stress in bone regions that are underloaded when using the reference Titanium alloy, therefore confirming that it could help to minimize stress-shielding effects (Fig 7). In particular, the stress transmission at the BII is significantly improved when considering high waviness ratios and high BIC ratios. Indeed, the distance where bone is in contact with the implant is higher for high waviness and BIC ratios, so that minimizing the gap of mechanical properties between the two materials is more effective to reduce stress shielding. It can be noted that in the present study, the standard Ti-6Al-4V alloy (E=113 GPa) was replaced by the metal-polymer composite Ti-35BPA (E=20GPa), which corresponds to a decrease of 82% of E. Ti-35BPA is specifically designed to match the bone stiffness [49]. This configuration represents an ideal situation where the implant and the bone are modeled with the same material, so that the stress distribution is only affected by the porosity of the osseointegrating BII (*i.e.* the void region in Fig 1b) and not by the gap of material properties at the BII.

4.4. An equivalent interphase

The proposed approach to determine the equivalent shear modulus of the BII could be used to describe the complex behavior of the BII in future FE studies. In this model, the interphase is represented by a homogeneous layer that does not include any geometrical roughness per se, but whose mechanical properties depend on the geometrical and material properties of the BII (*i.e.* on Δ/λ, on the BIC ratio and on E_b), therefore allowing to consider the microscopic properties of the BII at the macroscale without significantly increasing computation times. Moreover, different bone properties could be considered at the microscale (*i.e.* for the equivalent interphase) and at the macroscale (*i.e.* for the rest of the bone tissue), which is of interest to model bone remodeling phenomena.

Similar models of an equivalent BII had been developed in the literature, but considered tensile [52] or dynamic loadings [24], and did not account for shear loading configurations, which are however important in clinical practice for example in spinal [41] or hip implants [65]. In these previous studies, the equivalent interphase was modelled through its stiffness, that had similar variations as a function of the BIC, of E_b and of Δ/λ as in the present study. In particular, Raffa et *al.* [52] showed that when subjected to tensile loading, low BIC ratios strongly influenced the BII stiffness at the microscopic scale (i.e. for low values of Δ/λ), and high BIC ratios at the macroscopic scale (i.e. for high values of Δ/λ), which is in agreement with Fig 8a. This previous study also noticed a linear dependence of the interphase stiffness on E_b, which is in agreement with results obtained in Fig 8b.

4.5 Limitations

This study has several limitations. The implant surface roughness was described as sinusoidal, similarly as in previous papers [24, 26, 53]. This constitutes a strong approximation, especially at the microscopic scale, and considering real implant roughness profiles could lead to different results. In particular, the presence of low stress regions evidenced around $\tilde{x} = 0.5$ (Fig 2 and 5) might be affected by this assumption. However, a good agreement between models with sinusoidal and real implant roughness profiles measured by profilometry was obtained under dynamic loading in a previous study [23]. Furthermore, arbitrary irregular profiles could be generated by combining different sinusoidal profiles. Microscopic and macroscopic scale of the implant roughness were also considered separately in order to distinguish their respective effects on the stress distribution at the BII, while they would be combined in real configurations. Note that interpretation in terms of absolute value of the stress field should be made with caution because the amplitude of the stress field within the periprosthetic bone is directly proportional to the value of d.

Different approximations were made to simplify the model. In particular, a 2D model was considered herein to decrease associated calculation costs. While newly-formed bone tissue is known to be heterogeneous and viscoelastic [63], bone material properties were assumed to be homogeneous, isotropic and linearly elastic in our study. In particular, such assumption simplifies the microstructure of bone, which may include multiscale cavities in real configurations [16]. Moreover, a sharp edge was considered at the boundary between bone, the implant and soft tissue, which leads to local stress concentration. We chose not to chamfer the contact corner of bone tissue in order to keep a simple and standardized configuration. However, chamfering the contact corner may weaken this stress concentration and hence modify the stress field close to the BII. Due to the Saint-Venan principle, such modification is not likely to modify the stress field far from the BII. Note that it remains difficult to determine the shape of the chamfer due to the lack of experimental data, which explains why this point is left to future studies. Finally, adhesion phenomena, which can be significant at the beginning of the osseointegration process [28, 54], were neglected.

Conclusion

Under shear loading, two possible phenomena that may lead to bone resorption through stress-shielding are evidenced in this study, namely excessive interfacial shear stress in bone tissue directly in contact with the implant, and a poor transmission of shear stress to newly formed bone tissue partially surrounded by non-mineralized tissue. Overall, the stress distribution at the bone-implant interface (BII) is affected by the presence of an implant up to a distance of around 80% of the wavelength of the implant roughness, which defines a region of interest where stress-shielding is likely to occur. In particular, stress-shielding effects increase when the BIC ratio decreases, which further highlights the importance of maximizing the BIC to enhance the clinical success of endosseous implants. Moreover, stress-shielding can be reduced by choosing an implant material with mechanical properties close to those of the bone tissue. This study also

proposes to model the BII conditions through a shear modulus value that depends on the bone and the implant mechanical properties, on the BIC ratio and on the implant roughness. This simple model could be used to simplify the complex mechanical behavior of the BII in future FE studies.

Acknowledgements

This project has received funding from Paris Ile-de-France Region (DIM “Respore” and F2M Federation), from the CNRS through the MITI interdisciplinary program and from the European Research Council (ERC) under the European Union’s Horizon 2020 research and innovation program (grant agreement No 682001, project ERC Consolidator Grant 2015 BoneImplant).

Conflict of interest

The authors declare no competing interests.

References

[1] H. Abuhussein, G. Pagni, A. Rebaudi, and H. L. Wang, "The effect of thread pattern upon implant osseointegration," *Clin Oral Implants Res,* vol. 21, pp. 129-36, Feb 2010.

[2] T. Albrektsson, P. I. Brånemark, H.-A. Hansson, and L. Jj, "Osseointegrated Titanium Implants: Requirements for Ensuring a Long-Lasting, Direct Bone-to-Implant Anchorage in Man," *Acta orthopaedica Scandinavica,* vol. 52, pp. 155-70, 02/01 1981.

[3] R. K. Alla, K. Ginjupalli, N. Upadhya, S. Mohammed, R. sekar, and R. Ravi, "Surface Roughness of Implants: A Review," *Trends in Biomaterials and Artificial Organs,* vol. 25, pp. 112-118, 05/29 2011.

[4] S. Arabnejad, B. Johnston, M. Tanzer, and D. Pasini, "Fully porous 3D printed titanium femoral stem to reduce stress-shielding following total hip arthroplasty," *J Orthop Res,* vol. 35, pp. 1774-1783, Aug 2017.

[5] A. G. Au, V. James Raso, A. B. Liggins, and A. Amirfazli, "Contribution of loading conditions and material properties to stress shielding near the tibial component of total knee replacements," *Journal of Biomechanics,* vol. 40, pp. 1410-1416, 2007/01/01/ 2007.

[6] W. D. Bugbee, W. J. Culpepper, 2nd, C. A. Engh, Jr., and C. A. Engh, Sr., "Long-term clinical consequences of stress-shielding after total hip arthroplasty without cement," *J Bone Joint Surg Am,* vol. 79, pp. 1007-12, Jul 1997.

[7] D. Buser, S. Ingimarsson, K. Dula, A. Lussi, H. Hirt, and U. Belser, "Long-Term Stability of Osseointegrated Implants in Augmented Bone: A 5-Year Prospective Study in Partially Edentulous Patients," *The International journal of periodontics & restorative dentistry,* vol. 22, pp. 109-17, 05/01 2002.

[8] D. Y. Chong, U. N. Hansen, and A. A. Amis, "Analysis of bone-prosthesis interface micromotion for cementless tibial prosthesis fixation and the influence of loading conditions," *J Biomech,* vol. 43, pp. 1074-80, Apr 19 2010.

[9] E. W. Cole, S. G. Moulton, R. Gobezie, A. A. Romeo, J. B. Walker, E. Lederman, *et al.*, "Five-year radiographic evaluation of stress shielding with a press-fit standard length humeral stem," *JSES Int,* vol. 4, pp. 109-113, Mar 2020.

[10] A. Completo, F. Fonseca, and J. A. Simões, "Strain shielding in proximal tibia of stemmed knee prosthesis: experimental study," *J Biomech*, vol. 41, pp. 560-6, 2008.

[11] J. Duyck, L. Corpas, S. Vermeiren, T. Ogawa, M. Quirynen, K. Vandamme, *et al.*, "Histological, histomorphometrical, and radiological evaluation of an experimental implant design with a high insertion torque," *Clin Oral Implants Res*, vol. 21, pp. 877-84, Aug 2010.

[12] C. A. Engh, Jr., A. M. Young, C. A. Engh, Sr., and R. H. Hopper, Jr., "Clinical consequences of stress shielding after porous-coated total hip arthroplasty," *Clin Orthop Relat Res*, pp. 157-63, Dec 2003.

[13] K. Firoozbakhsh and M. Aleyaasin, "The effect of stress concentration on bone remodeling: theoretical predictions," *J Biomech Eng*, vol. 111, pp. 355-60, Nov 1989.

[14] M. Fraulob, S. Pang, S. Le Cann, R. Vayron, M. Laurent-Brocq, S. Todatry, *et al.*, "Multimodal characterization of the bone-implant interface using Raman spectroscopy and nanoindentation," *Med Eng Phys*, vol. 84, pp. 60-67, Oct 2020.

[15] M. Fraulob, R. Vayron, S. Le Cann, B. Lecuelle, Y. Hériveaux, H. Albini Lomami, *et al.*, "Quantitative ultrasound assessment of the influence of roughness and healing time on osseointegration phenomena," *Sci Rep*, vol. 10, p. 21962, Dec 15 2020.

[16] A. Fritsch and C. Hellmich, "'Universal' microstructural patterns in cortical and trabecular, extracellular and extravascular bone materials: Micromechanics-based prediction of anisotropic elasticity," *Journal of Theoretical Biology*, vol. 244, pp. 597-620, 2007/02/21/ 2007.

[17] H. M. Frost, "A 2003 update of bone physiology and Wolff's Law for clinicians," *Angle Orthod*, vol. 74, pp. 3-15, Feb 2004.

[18] F. Galloway, M. Kahnt, H. Ramm, P. Worsley, S. Zachow, P. Nair, *et al.*, "A large scale finite element study of a cementless osseointegrated tibial tray," *Journal of Biomechanics*, vol. 46, pp. 1900-1906, 2013/07/26/ 2013.

[19] X. Gao, M. Fraulob, and G. Haïat, "Biomechanical behaviours of the bone-implant interface: a review," *J R Soc Interface*, vol. 16, p. 20190259, Jul 26 2019.

[20] M. Gortchacow, M. Wettstein, D. P. Pioletti, and A. Terrier, "A new technique to measure micromotion distribution around a cementless femoral stem," *J Biomech*, vol. 44, pp. 557-60, Feb 3 2011.

[21] S. Gupta, N. Patil, J. Solanki, R. Singh, and S. Laller, "Oral Implant Imaging: A Review," *The Malaysian journal of medical sciences : MJMS*, vol. 22, pp. 7-17, May-Jun 2015.

[22] G. Haïat, H.-L. Wang, and J. Brunski, "Effects of Biomechanical Properties of the Bone–Implant Interface on Dental Implant Stability: From In Silico Approaches to the Patient's Mouth," *Annual Review of Biomedical Engineering*, vol. 16, pp. 187-213, 2014.

[23] Y. Hériveaux, V.-H. Nguyen, V. Brailovski, C. Gorny, and G. Haiat, "Reflection of an ultrasonic wave on the bone−implant interface: Effect of the roughness parameters," *The Journal of the Acoustical Society of America*, vol. 145, 06/01 2019.

[24] Y. Hériveaux, V. H. Nguyen, S. Biwa, and G. Haïat, "Analytical modeling of the interaction of an ultrasonic wave with a rough bone-implant interface," *Ultrasonics*, vol. 108, p. 106223, Dec 2020.

[25] Y. Heriveaux, V. H. Nguyen, V. Brailovski, C. Gorny, and G. Haiat, "Reflection of an ultrasonic wave on the bone-implant interface: Effect of the roughness parameters," *J Acoust Soc Am*, vol. 145, p. 3370, Jun 2019.

[26] Y. Heriveaux, V. H. Nguyen, and G. Haiat, "Reflection of an ultrasonic wave on the bone-implant interface: A numerical study of the effect of the multiscale roughness," *J Acoust Soc Am*, vol. 144, p. 488, Jul 2018.

[27] R. Huiskes, H. Weinans, and B. van Rietbergen, "The relationship between stress shielding and bone resorption around total hip stems and the effects of flexible materials," *Clin Orthop Relat Res*, pp. 124-34, Jan 1992.

[28] K. Immel, T. X. Duong, V.-H. Nguyen, G. Haïat, and R. A. Sauer, "A modified Coulom, s law for the tangential debonding of osseointegrated implants," *Biomechanics and Modeling in Mechanobiology,* vol. 19, pp. 1091-1108, 2020.

[29] R. Jimenez, "The Radiology of Orthopaedic Implants. An Atlas of Techniques and Assessment," *The Journal of Bone and Joint Surgery-American Volume,* vol. 84, p. 514, 03/01 2002.

[30] C. B. Johansson and T. Albrektsson, "Integration of screw implants in the rabbit: a 1-year follow-up of removal torque of titanium implants," *The International journal of oral & maxillofacial implants,* vol. 2 2, pp. 69-75, 1987.

[31] M. G. Joshi, S. G. Advani, F. Miller, and M. H. Santare, "Analysis of a femoral hip prosthesis designed to reduce stress shielding," *J Biomech,* vol. 33, pp. 1655-62, Dec 2000.

[32] N. Kohli, J. C. Stoddart, and R. J. van Arkel, "The limit of tolerable micromotion for implant osseointegration: a systematic review," *Scientific Reports,* vol. 11, p. 10797, 2021/05/24 2021.

[33] R. Korabi, K. Shemtov-Yona, A. Dorogoy, and D. Rittel, "The Failure Envelope Concept Applied To The Bone-Dental Implant System," *Sci Rep,* vol. 7, p. 2051, May 17 2017.

[34] J. Kuiper and R. Huiskes, "The Predictive Value of Stress Shielding for Quantification of Adaptive Bone Resorption Around Hip Replacements," *Journal of biomechanical engineering,* vol. 119, pp. 228-31, 09/01 1997.

[35] D. Kurniawan, F. M. Nor, H. Y. Lee, and J. Y. Lim, "Finite element analysis of bone-implant biomechanics: refinement through featuring various osseointegration conditions," *Int J Oral Maxillofac Surg,* vol. 41, pp. 1090-6, Sep 2012.

[36] T. Kusano, T. Seki, Y. Higuchi, Y. Takegami, Y. Osawa, and N. Ishiguro, "Preoperative Canal Bone Ratio is Related to High-Degree Stress Shielding: A Minimum 5-Year Follow-Up Study of a Proximally Hydroxyapatite-Coated Straight Tapered Titanium Femoral Component," *J Arthroplasty,* vol. 33, pp. 1764-1769, Jun 2018.

[37] S. Le Cann, E. Tudisco, C. Perdikouri, O. Belfrage, A. Kaestner, S. Hall, *et al.*, "Characterization of the bone-metal implant interface by Digital Volume Correlation of in-situ loading using neutron tomography," *Journal of the Mechanical Behavior of Biomedical Materials,* vol. 75, 07/01 2017.

[38] M.-J. Li, P.-C. Kung, Y.-W. Chang, and N.-T. Tsou, "Healing Pattern Analysis for Dental Implants Using the Mechano-Regulatory Tissue Differentiation Model," *International Journal of Molecular Sciences,* vol. 21, p. 9205, 12/02 2020.

[39] Y. J. B. Manikyamba, S. S. Mc, A. V. R. Raju, B. Rao, and C. K. Nair, "Implant thread designs: An overview," 2018.

[40] V. Mathieu, R. Vayron, G. Richard, G. Lambert, S. Naili, J. P. Meningaud, *et al.*, "Biomechanical determinants of the stability of dental implants: influence of the bone-implant interface properties," *J Biomech,* vol. 47, pp. 3-13, Jan 3 2014.

[41] A. D. Melnyk, T. L. Wen, S. Kingwell, J. D. Chak, V. Singh, P. A. Cripton, *et al.*, "Load transfer characteristics between posterior spinal implants and the lumbar spine under anterior shear loading: an in vitro investigation," *Spine (Phila Pa 1976),* vol. 37, pp. E1126-33, Aug 15 2012.

[42] A. Michel, R. Bosc, J. P. Meningaud, P. Hernigou, and G. Haiat, "Assessing the Acetabular Cup Implant Primary Stability by Impact Analyses: A Cadaveric Study," *PLoS One,* vol. 11, p. e0166778, 2016.

[43] S. Mondal and R. Ghosh, "Effects of implant orientation and implant material on tibia bone strain, implant-bone micromotion, contact pressure, and wear depth due to total ankle replacement," *Proc Inst Mech Eng H,* vol. 233, pp. 318-331, Mar 2019.

[44] E. F. Morgan, G. U. Unnikrisnan, and A. I. Hussein, "Bone Mechanical Properties in Healthy and Diseased States," *Annu Rev Biomed Eng,* vol. 20, pp. 119-143, Jun 4 2018.

[45] A. N. Natali, P. G. Pavan, and A. L. Ruggero, "Analysis of bone-implant interaction phenomena by using a numerical approach," *Clin Oral Implants Res,* vol. 17, pp. 67-74, Feb 2006.

[46] J. W. Nicholson, "Titanium Alloys for Dental Implants: A Review," 2020.

[47] M. Niinomi and M. Nakai, "Titanium-Based Biomaterials for Preventing Stress Shielding between Implant Devices and Bone," *International journal of biomaterials,* vol. 2011, p. 836587, 06/22 2011.

[48] I. V. Okulov, A. S. Volegov, H. Attar, M. Bönisch, S. Ehtemam-Haghighi, M. Calin, *et al.*, "Composition optimization of low modulus and high-strength TiNb-based alloys for biomedical applications," *Journal of the Mechanical Behavior of Biomedical Materials,* vol. 65, pp. 866-871, 2017/01/01/ 2017.

[49] I. V. Okulov, J. Weissmüller, and J. Markmann, "Dealloying-based interpenetrating-phase nanocomposites matching the elastic behavior of human bone," *Scientific Reports,* vol. 7, p. 20, 2017/02/02 2017.

[50] G. Orsini, B. Assenza, A. Scarano, M. Piattelli, and A. Piattelli, "Surface analysis of machined versus sandblasted and acid-etched titanium implants," *Int J Oral Maxillofac Implants,* vol. 15, pp. 779-84, Nov-Dec 2000.

[51] C. Piao, D. Wu, M. Luo, and H. Ma, "Stress shielding effects of two prosthetic groups after total hip joint simulation replacement," *Journal of Orthopaedic Surgery and Research,* vol. 9, p. 71, 2014/08/30 2014.

[52] M. L. Raffa, V. H. Nguyen, and G. Haiat, "Micromechanical modeling of the contact stiffness of an osseointegrated bone-implant interface," *Biomed Eng Online,* vol. 18, p. 114, Dec 3 2019.

[53] M. L. Raffa, V. H. Nguyen, P. Hernigou, C. H. Flouzat-Lachaniette, and G. Haiat, "Stress shielding at the bone-implant interface: Influence of surface roughness and of the bone-implant contact ratio," *J Orthop Res,* vol. 39, pp. 1174-1183, Jun 2021.

[54] J. Rojek and J. J. Telega, "Numerical simulation of bone-implant systems using a more realistic model of the contact interfaces with adhesion," *Journal of Theoretical and Applied Mechanics,* vol. 37, pp. 659-686, 1999.

[55] H. J. Rønold and J. E. Ellingsen, "Effect of micro-roughness produced by TiO2 blasting--tensile testing of bone attachment by using coin-shaped implants," *Biomaterials,* vol. 23, pp. 4211-9, Nov 2002.

[56] F. Rupp, L. Liang, J. Geis-Gerstorfer, L. Scheideler, and F. Hüttig, "Surface characteristics of dental implants: A review," *Dent Mater,* vol. 34, pp. 40-57, Jan 2018.

[57] H. S. Ryu, C. Namgung, J. H. Lee, and Y. J. Lim, "The influence of thread geometry on implant osseointegration under immediate loading: a literature review," *J Adv Prosthodont,* vol. 6, pp. 547-54, Dec 2014.

[58] A. M. Sadegh, G. M. Luo, and S. C. Cowin, "Bone ingrowth: An application of the boundary element method to bone remodeling at the implant interface," *Journal of Biomechanics,* vol. 26, pp. 167-182, 1993/02/01/ 1993.

[59] A. Shirazi-Adl, M. Dammak, and G. Paiement, "Experimental determination of friction characteristics at the trabecular bone/porous-coated metal interface in cementless implants," *J Biomed Mater Res,* vol. 27, pp. 167-75, Feb 1993.

[60] D. R. Sumner, "Long-term implant fixation and stress-shielding in total hip replacement," *J Biomech,* vol. 48, pp. 797-800, Mar 18 2015.

[61] T. Tang, V. Ebacher, P. Cripton, P. Guy, H. McKay, and R. Wang, "Shear deformation and fracture of human cortical bone," *Bone,* vol. 71, pp. 25-35, Feb 2015.

[62] C. H. Turner, T. Wang, and D. B. Burr, "Shear strength and fatigue properties of human cortical bone determined from pure shear tests," *Calcif Tissue Int,* vol. 69, pp. 373-8, Dec 2001.

[63] R. Vayron, M. Matsukawa, R. Tsubota, V. Mathieu, E. Barthel, and G. Haiat, "Evolution of bone biomechanical properties at the micrometer scale around titanium implant as a function of healing time," *Phys Med Biol,* vol. 59, pp. 1389-406, Mar 21 2014.

[64] R. Vayron, V.-H. Nguyen, B. Lecuelle, H. Albini Lomami, J.-P. Meningaud, R. Bosc, *et al.*, "Comparison of Resonance Frequency Analysis and of Quantitative Ultrasound to Assess Dental Implant Osseointegration," *Sensors (Basel, Switzerland)*, vol. 18, p. 1397, 05/02 2018.

[65] C. Voigt, C. Klöhn, R. Bader, G. von Salis-Soglio, and R. Scholz, "Finite element analysis of shear stresses at the implant-bone interface of an acetabular press-fit cup during impingement," *Biomed Tech (Berl)*, vol. 52, pp. 208-15, Apr 2007.

[66] H. Weinans, D. R. Sumner, R. Igloria, and R. N. Natarajan, "Sensitivity of periprosthetic stress-shielding to load and the bone density-modulus relationship in subject-specific finite element models," *J Biomech*, vol. 33, pp. 809-17, Jul 2000.

[67] G. Yamako, D. Janssen, S. Hanada, T. Anijs, K. Ochiai, K. Totoribe, *et al.*, "Improving stress shielding following total hip arthroplasty by using a femoral stem made of β type Ti-33.6Nb-4Sn with a Young's modulus gradation," *J Biomech*, vol. 63, pp. 135-143, Oct 3 2017.

[68] Q.-H. Zhang, A. Cossey, and J. Tong, "Stress shielding in periprosthetic bone following a total knee replacement: Effects of implant material, design and alignment," *Medical Engineering & Physics*, vol. 38, 10/01 2016.

[69] Y. Zhou, C. Gong, M. Hossaini-Zadeh, and J. Du, "3D Contact and Strain in Alveolar Bone Under Tooth/Implant Loading," in *TMS 2019 148th Annual Meeting & Exhibition Supplemental Proceedings*, Cham, 2019, pp. 793-798.